Materials Physics and Chemistry (2022) Volume 4, No 1
doi:10.18282/mpc.v1i1.570

Original Research Article

Numerical simulation of macrosegregation impurities in the solidifying continuous casting steel billet

O.V. Hress[1]*, O.B. Isayev[1], O.O. Chebotaryova[2], Kaiming Wu[1]

[1]The State Key Laboratory for Refractories and Metallurgy, Hubei Province Key Laboratory of Systems Science in Metallurgical Process, International Research Institute for Steel Technology, Wuhan University of Science and Technology, Wuhan 430081, China
[2]Dneprovsky State Technical University, 2, Dneprostroyevskaya, Kam'anske, Dnepropetrovsk region. 51900, Ukraine
**Correspondence: agress@ua.fm*

ABSTRACT

In this study, new theoretical conceptions have been developed about an impurity segregation mechanism at the time of alloy solidification considering present microvolumes with different chemical compositions during alloy solidification. It has been concluded that this conception allows to establish and optimize technologic parameters that influence the production of the main types of macro-heterogeneity. The derived model conceptions have confirmed the final condition of real continuous casting billets by using the advanced analyzing methods.

Highlights

- The quasi-equilibrium theory used to study the hardening processes of alloys has been expanded and improved.
- The development of a numerical model for macrosegregation impurities in solidifying continuous casting billet is suggested.
- The adequacy of the developed model is checked under the industrial conditions using comparison theoretical
- calculations and practical data.
- The results and developments that are obtained are discussed.

Keywords: *steel; solidification; macrosegregation; numerical simulation; continuous casting.*

Received: Nov 24, 2021 **Accepted:** Dec 26, 2021 **Online:** Jan 14, 2022

1. Introduction

Practically, all properties of the metal are associated with metal solidification and predetermine the impurity distribution in a solidified alloy. The time numerical simulation of solidification associated with heat-mass exchange inside the mushy zone of alloys is a predominant investigation method as the physical methods of investigations are imperfect. The existing mathematical models for alloys apply different methods to determine the formed solid-phase quantity as a rule. In these cases, the time-dependent thermal conductivity can be applied in Stephen task, equilibrium, nonequilibrium, or quasi-equilibrium models. The Stephen model is used for a simple task only when the solidified alloy has small mushy zones. These conditions are considered typical for pure metals and small size ingots with high thermal conductivity.

Generally, the equilibrium model is used for relatively low cooling speed, the high mobility of alloying elements in the liquid melt, and highly dispersed structure of ingot. These conditions are not always applicable in the case of continuous casting especially. The quasi-equilibrium theory is one of the advanced theories used for alloy solidification that describes heat processes into solidified ingots quite simply and appropriately [1]. This theory neglects overcooling inside the mushy zone. In this case, the heat of phase transition that produces the mushy zone of the solidified metal can be set by the smoothed or effective specific heat dependence of temperature. At the same time, the quasi-equilibrium theory of the mushy zone has the following limitations:

1. This theory does not consider the change in the coefficient impurity distribution during the solidification process. In fact, the change in the coefficient impurity distribution is associated with the solidification speed, free energies of alloys and solid crystals, and impure chemical potential in solid and liquid phases and temperature of course [2,3].

2. This theory reduces the function of liquid hydrodynamic motion inside the mushy zone to effectively increase the diffusion coefficient. This assumption considers different propositions for exponential types of impurities and temperature distributions into a diffusional layer in all mushy zone [4–6]. This assumption considers smooth and synchronous changes in segregating distribution across the mushy zone width.

3. The numerical realization in the quasi-equilibrium theory considers the dependence of the liquid phase section on the distribution coefficient one impurity but in reality, many chemical elements of the alloy segregate.

Therefore, this model does not allow to predict the formation of macroperiodical structures in a solidified alloy with full measure. We found that the periodical solidification of steel and the macroperiodical impurity distribution in a solid ingot was first described by Gugcov [7] and Dudovcev [8] and thereafter have been discussed in many other research works. The mechanism of the formation of periodical structures has not yet determined in detail. Generally, the development of solidification processes is presented as periodical solidification of front-edge movement and as a result of the periodically solidified front edge is influenced by the change in density and mechanical and hydrodynamic properties [9–11].

Later researchers started studying melt motion inside the mushy zone that possesses a capillary-porous medium due to the capillary effect. The Darcy law describes liquid motion in this medium. Mehrabian *et al*. [12] attempted the first time to describe the movement of segregates during solidification. The most advanced model was presented by Ni and Beckermann [13]. This model allows calculating the liquid motion inside liquid that is free from crystals and inside the mushy zone. However, the numerical realization of this model for solidification of continuous casting at a full scale demands the advanced high-tech highly productive computers with large memory space. This is not considered as a reasonable process in some cases. In addition, if different speeds of segregates are not considered, it results in impure periodical co-phasal accumulation into the particular zones from ingots periphery to center.

It was pointed out earlier [14,15] that different chemical elements have different concentration extrema in the time and space because segregates have different moving speeds into the mushy zone. In the first place, the speed of impurities depends on the concentration of chemical elements [16]. In addition, the chemical segregation of elements does not depend on solidification periodicity [17]. After analyzing the above-mentioned concepts and literature data [18–21], we note the absence of the harmonious mechanism for models based on the mathematical manipulation to prove different speeds of segregates for experimental data because it is a very complicated phenomenon.

2. Investigation objective

To develop a solidification method which alloys with different chemical compositions by using considering various macrogroups of atoms with different chemical compositions in a solidifying melt.

3. Materials and methods

We consider the following premise for a new mathematical model to segregate impurities:

1. Three zones are formed inside the billet during segregation (**Figure 1**): solid metal zone, mushy zone, and liquid zone (core).
2. The diffusion into the solid phase can be neglected because the values of coefficients are very small.
3. The mushy zone is a dendrite complex directed to the isoliquidus line.
4. The motion of matric melts with different quantities of segregates as compared with a solid phase takes part between dendrite needles. The correlation between impurities in the solid phase and the matrix melt is different for every impurity and depends on their initial concentrations.

5. The diffusion of impurities inside the matrix melt has finite quantity.

6. Capillary presser and dissolved gas emission induce matrix melt motion inside the mushy zone. We do not consider thermo-filtration and convective parts because of the low speed of mixing of matrix melts and low-temperature gradient in the mushy zone.

7. Capillary presser depends on the distance between dendrites' arms and surface tension on the border of melted crystal. The surface tension depends on the activity ratio of every segregate, which considers the concentration of other impurities in the melt.

8. The geometrical place of the calculated cell with the solid phase value of 80-85% defines the internal billet shell position. The border of the mushy zone has 20-25% of the solid phase.

9. In the mushy zone border, the liquid phase core instantly takes away impurities with averaging inside liquid phase.

10. Convective mixing of the main liquid masses of the solidified billet has thermo-gravitational characteristics as no solidified parts of the billet take more time than the billet section and submerged entry nozzle stream penetration depth.

11. Chemical reactions and peritectic transformation are absent.

12. The heat flux along the technological axis is absent.

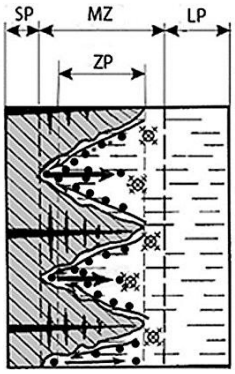

Fig. 1. The scheme of segregates filtration in the mushy zone:
SP–solid phase, MZ–mushy zone, LP–liquid phase, ZP–filtration zone.

Accordingly, the model equation of thermal conductivity in the solid and the mushy zone is expressed as follows:

$$\frac{\partial[(c_s\rho_s - c_l\rho_l)\xi + c_l\rho_l]\cdot t}{\partial\tau} + Q = \nabla[(\lambda_s - \lambda_l)\xi + \lambda_l]\nabla t + L\rho_s\frac{\partial\xi}{\partial\tau}$$

where ρ_s, ρ_l, c_s, c_l, λ_s, λ_l are the density, thermal conductivity, thermal conduction of solid (s) and liquid (l) metals, respectively; L is the heat of phase transition; τ is the time; t is the temperature; ξ is the relative part of the solid phase; and Q is the heat flux volume density.

The steel density is constant and the liquid steel density depends on temperature and the concentration of impurities. The thermal capacity and thermal conductivity of liquid steel are constant, and the thermal capacity and thermal conductivity of the solid steel depends on temperature and the concentration of impurities.

The time numerical techniques of differential equation decision (finite-difference method and finite-element method) have widespread occurrence. The applications of these methods can decide tasks for any objects with arbitrary shape, every boundary condition, and the dependence of different thermophysical properties on temperature. One of the easiest and reliable methods is the control volume method [22]. The main feature of this method is the possibility of receiving the second-order finite-difference scheme for the inside rated operating conditions and the boundary.

Accordingly, the accepted assumption about the negligibly small heat flux and the speed of segregation impurities along the continuous caster technology axis for impurity segregation calculation used a two-dimensional model (axes X and Y). In our case, one-quarter of the solidified billet cross-section is rated as operating conditions. This decision is taken because inside the mold-liquid pool the solidification processes are symmetrical relative to billet cross-section axes. Then, the boundary conditions take form (1):

1. Initial conditions:

$$\tau = 0, t_n = t_{n,0} \qquad (2)$$

where $t_{n,0}$ is the initial temperature for *n* element (temperature distribution is uniform because when the metal gets into the mold the speed of c convection streams is very high).

2. Boundary conditions for the axes X and Y take the following form:

$$-\lambda \frac{\partial t}{\partial x}\Big|_{x=0} = 0, -\lambda \frac{\partial t}{\partial y}\Big|_{y=0} = 0. \qquad (3)$$

Quantity *Q* is associated with staying in the space of continuous casting billet under rated operating conditions. If rated operating conditions are on the interphase boundary (solid phase–environment or mushy zone–liquid core), the heat flux density is *Q* = α · gradt (hear and after α-summary heat transfer). In other cases, *Q* = 0.

On the interface boundaries, the α value can be obtained as follows. The heat flux from the external billet surface on the forced secondary cooling zone is calculated by using the real statistical dependence of the heat transfer coefficient on the water consumption for the continuous caster. For the mathematical model, the heat transfer outside the forced secondary cooling zone is submitted to the radiant–convection heat exchange:

$$-\lambda \frac{\partial T}{\partial n} = \alpha_k (T_{\text{surf}} - T_{\text{env}}) + \varepsilon \sigma_0 \left({T_{\text{surf}}}^4 - {T_{\text{env}}}^4 \right) \qquad (4)$$

where α_k is the convection heat exchange coefficient that depends on the cooled surface inside continuous caster space, ε is the body blackness degree, σ_0 is the Stephen–Boltzmann constant, and $T_{\text{surf}}, T_{\text{env}}$ are the surface temperature and environment temperature in K, respectively.

The Newton's method is used for the temperature definition in equation (4) considering the needle temperature location in the center of the calculated cells. The heat flux coefficient on the liquid metal pool is calculated by using the following equation:

$$\alpha = \frac{Nu \cdot \lambda_l}{l}, \qquad (5)$$

where Nu is taken from an earlier work [23] and the forced liquid motion induced by the submerged stream is found as $Nu = 5.0 + 0.021Pe$, and in other parts of the liquid pool without the submerged stream influence it is found as $Nu = 0.56(Gr \cdot Pr^2)^{0.25}$ (where Gr, Pr, and Pe are the Grasgof, Prandtl, and Peclet numbers, respectively, and l is the characteristic size).

The specific heat flux quantity Q from billet to mold wall is calculated by mathematical manipulation [24], which well correlates with data [25]. The mass change Δm of the solidified metal inside the elementary calculated space and in the solidification temperature range for the chosen steel grade is calculated according to the following formula:

$$\Delta m = \frac{(c_s \xi + c_l (1-\xi))(t^{n+1} - t^n)}{L + (c_l t_l - c_s t_s)} m \qquad (6)$$

where m is the calculated volume mass; t^{n+1} is the excess temperature inside the calculated point at the (n + 1) time interval. Obviously, if the difference between the previous temperature and the excess temperature is positive at the elementary calculated volume the solid mass increases, and if the difference is negative the solid mass decreases.

From calculations, it was accepted that the solid and liquid phase temperatures inside the mushy zone are equal to the solidus temperature (t_s) and the liquidus temperature (t_l) considering the current concentrations of the chemical elements. Then, the real temperature in the calculated point depends on the ratio of the solid and liquid phases:

$$t^{n+1} = \frac{t_l (1-\xi) c_l + t_s \xi c_s}{c_s \xi + c_l (1-\xi)} \qquad (7)$$

The process of the impurity transfer at the time of billet solidification can be described by the following diffusion equation [26]:

$$\frac{\partial C}{\partial \tau} = D_l \nabla [(1-\xi) \cdot \nabla C_l] - \xi V_l \nabla C_l; C = C_l (1-\xi) + C_s \xi \qquad (8)$$

where C is the concentration of the segregated chemical element; D_l, C_s, C_l are the diffusion coefficient and current concentration for every segregated impurity inside the solid phase and liquid melt, respectively; V_l is the matrix melt motion speed between dendrites arms in every calculated area of the mushy zone. The initial and boundary conditions in Eq. (8) are decided similar to Eqs. (2) and (3).

The quantity V_l is calculated by using the Darcy equation for the defined liquid speed of filtration through the capillary-porous medium as follows:

$$V_l = \frac{K\Delta P}{\mu l_{ZP}} \qquad (9)$$

where K is the penetrability coefficient for the filtration section, μ is the dynamic viscosity coefficient for the filtrated liquid, and ΔP is the pressure difference in the filtration zone.

The penetrability coefficient is calculated by the following formula [27]:

$$K = \frac{l_1 l_2}{24\pi c_0^3} \qquad (10)$$

Our statistical analysis depends on experimental data [23] as follows:

$$l_1 = 1.241 \cdot 10^{-5} R^{-0.29}; \qquad (11)$$

$$l_2 = 8.5 \cdot 10^{-6} R^{-0.466}, \qquad (12)$$

where is R is the cooling speed (K/c).

The quantity ΔP is calculated by the following formula:

$$\Delta P = \frac{4\sigma_{\mathrm{sl}}}{l_2} \pm \rho_l g H \cdot \sin\theta - (\rho_l - \rho_{\mathrm{av}}) \cdot g l_1 \qquad (13)$$

where σ_{sl} is the surface tension coefficient on the crystal–liquid boundary, H is the height of a liquid column above the calculated section, θ is the capillary canting angle, ρ_{av} is the melt density between dendrites. The sign ± depends on the capillary location on the upper or lower continuous caster radius, and g is the acceleration of gravity.

Presser solved gas forces are also considered in this model (forces defined by Siewert's low). When presser reaches certain critical level and liquid fracture then the model fixes pore formation and the segregate speed becomes equal to zero.

Considering different speeds of impurity segregation at the steel solidification time, this numerical model takes into account the liquid structure of quasi-chemical theoretical positions. In particular [23], it was assumed that liquid has different kinds of atomic microgroups with different chemical elemental shares, for example, microgroups with different carbon content, sulfa content, etc. These microgroups can unite to conglomerate. The conglomerates of microgroups are not steady, do not have distinct interphase boundaries, and interact with each other all times according to interatomic chemical interactions. In other words, metallic liquid properties can be estimated considering the changing activity coefficients of components according to additivity laws. Therefore, different segregation levels of chemical elements can explain the conglomerate motion of a microgroup in the inter-dendritic space of the mushy zone. Different conglomerates of a microgroup differ from one another in terms of the physical and chemical properties, for example, density, surface tension.

For calculating σ_{sl} for every i impurity with the above assumption, the following equation is used:

$$\sigma_{sl}^{i} = \sigma_0 - a_i ln(1 + b_i \gamma_i C_i), \qquad (14)$$

where σ_0 is the surface tension for the pure metal, a_i, b_i are different constants for every i^{th} chemical element with concentration C_i[1], and γ_i is the activity coefficient of the i^{th} element depending on other impurity concentrations in the melt.

[1] The calculation of these constants is authors' prerogative.

Segregated impurity quantities in the solid C_s and liquid C_l phases at the $(n + 1)$ time station inside the elementary volume are determined by using the following balance equations:

$$C_s^{n+1} = C_s^n m_s^n + K_{ef} C_l^n \Delta m; \quad (15)$$

$$C_l^{n+1} = C_{\text{av}}^n m - C_s^{n+1}, \quad (16)$$

where m_s and m are the solid phase mass and elementary volume mass, respectively, C_{av} is the average impurity quantity in the calculated cell, and K_{ef} is the efficient distribution coefficient in the present impurity.

If in the solid phase diffusion is absent, the quantity K_{ef} can be calculated by using the following expression [23,24]:

$$K_{\text{ef}} = \frac{C_s}{C_l} = \frac{K_0}{K_0 + (1 - K_0) e^{-V_{kr} \frac{\delta}{D_l}}} \quad (17)$$

where K_0 is the equilibrium distribution coefficient that depends on the impurity concentration, for example, for the calculation of sulfur segregation as used earlier [23], the statistical dependence is found to be $K_0 = 0.077 + 0.175[S]^{0.52}$), V_{kr} is the solidification frontal zone motion speed, and δ is the diffusion layer thickness. As shown earlier (17), evidently the quantity K_{ef} is first defined by the dimensionless parameter $V_{\text{kr}} \frac{\delta}{D_l}$. According to Sladcoshteev et al. [25], the diffusion mobility quantity δ / D_l is defined by using the solidification speed weakly. Accordingly, the diffusion mobility can be calculated by K_{ef} experimental data.

The explanation is based on the example of carbon. According to an earlier study [29], the carbon diffusion mobility at ingot solidification time is 0.12×10^5 s/m and practically it does not change for the carbon concentration interval 0.15–0.73%. Therefore, if the amount D_l is known, the calculation of the thickness of the diffusion liquid phase layer adjacent to interface is not difficult. This quantity is found to be near 3.5×10^{-4} m, which is close to data [27,31,32]. The small amounts δ confirms that the impurity transfer inside the mushy zone is determined not only by diffusion but also by the filtration mass transfer. Then, assuming that the diffusion layer thickness is constant for all segregated impurities, the quantity δ / D_l can be calculated for sulfur and it is not difficult to calculate for other segregates as well.

The developed model adequacy is examined under the industrial conditions. The continuous casting billet surface is measured after mold and in the secondary cooling zone by accepted pyrometers by using the standard method. The segregated impurity quantity in the billet sections is defined by chemical analyses along the axes and diagonal transversal templates by using the standard method. **Figure 2** shows section 335 × 400 mm of the billet transverse template with sampling pattern as an example. Active numerical experiments and results are determined by using the mathematical and statistical methods. The confidence level for all calculations was found to be 95%. All coefficients found in the regression equations were statistically significant.

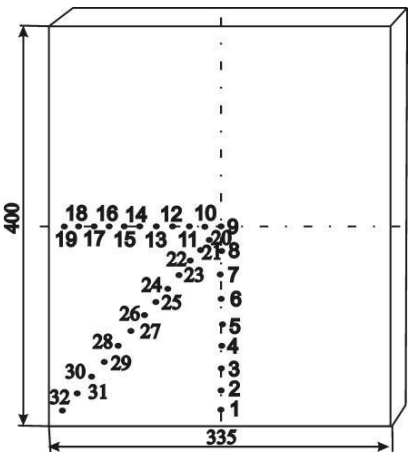

Fig. 2. Section 335 × 400 mm of billet transversal template with sampling pattern.

3. Results and discussion

The next continuous casting basic parameters used for calculations are as follows: mold height: 1 m; forced secondary cooling zone length: 6.28 m (first zone: 0.4 m; second: 0.95 m; third: 1.82 m; forth: 3.11 m); the distance from metal meniscus to the first withdrawal roll set: 13.169 m; distance to the beginning of the strengthening zone: 19.4 m; distance to the ending of the strengthening zone: 24.3 m; continuous caster basic radius: 14 m; continuous caster metallurgical length: 33 m.

The results of solidification calculations and real temperature measured with average data for billet with section335 × 400 mm of the upper radius surface are presented in Figure 3. The temperature of the upper radius surface is measured after mold, in the secondary cooling zone boundaries, and later along the continuous caster technological axis. The average casting speed for 20 heat sequence of steel grade 20 (chemical composition is presented in Table 1) was found to be 0.6 m/min.

Table 1. Chemical composition, mass%. Steel 20 (GOST 1050–88).

C	Si	Mn	Ni	S	P	Cr	Cu	As
0.17–0.24	0.17–0.37	0.35–0.65	≤0.25	≤0.04	≤0.04	≤0.25	≤0.25	≤0.08

The next symbols are presented in **Figure 3**: t_{surf}: temperature in the center of the bill*et al*ong wide side; G_w: water consumption for the secondary cooling segment. We found that the developed mathematical model under cooling billet thermal conditions is adequate to real conditions with a relative error of less than 3%. We compared chemical analysis data using transversal templates with calculated data using mathematical statistics. The matching probability varied from 61.4% to 94.6% for carbon and from 68.4% to 73.8% for sulfur.

The graphical comparison segregating elemental distribution across the section for billet 335 × 400 mm of steel grade 45 according to GOST 1050–88 between the calculated and experimental data is presented in **Figure 4.** This distribution allows to visually estimate impurity segregation character along the billet axes and diagonal (numeration of control points is similar to Figure 2). The matching probability for every compared calculation was less than 5.3% for carbon distribution and less than 9.8% for sulfur segregation.

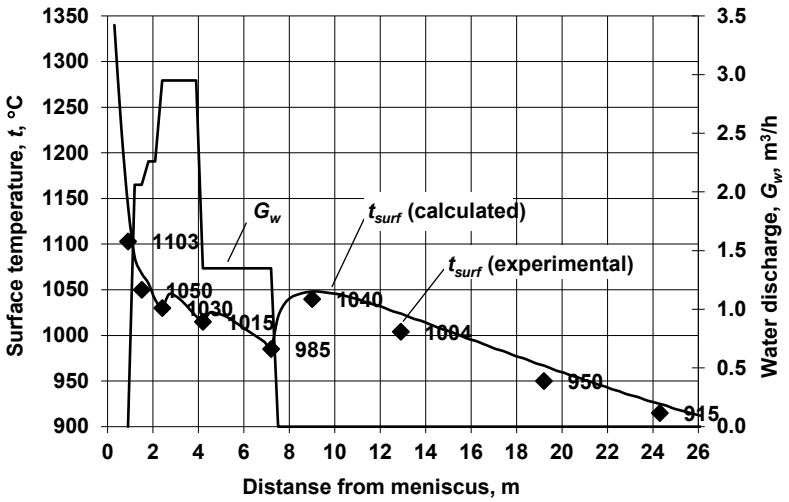

Fig. 3. Calculated and experimental data comparison around temperature distribution along CC technological axes.

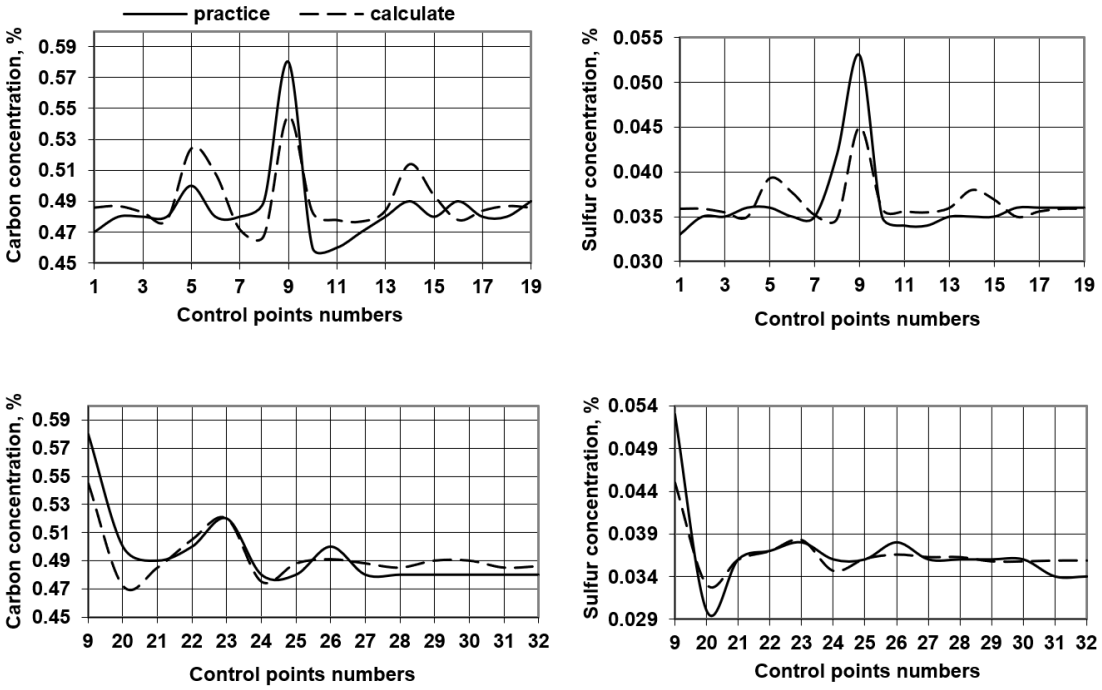

Fig. 4. Graphs of billets template segregate distribution along axes and diagonal.

The calculated results for the desired parameter distribution for billet transverse sections across the mushy zone width are presented in Figures 5 and 6. The initial contents were 0.04% for sulfur and 0.1% for carbon. Other conditions were the same: t_{aver}, t_{llikph}, t_{slikph}, t_{lsolph},: melt average temperature, solidus and liquidus temperatures for the liquid phase, solidus and liquidus temperatures for the solid phase, respectively; D_{solph}: solid phase share;%; KS_{likph}, KS_{solph}: sulfur segregation coefficients in the liquid and solid phases, respectively; KC_{likph}, KC_{solph}: carbon segregation coefficients in the liquid and solid phases, respectively.

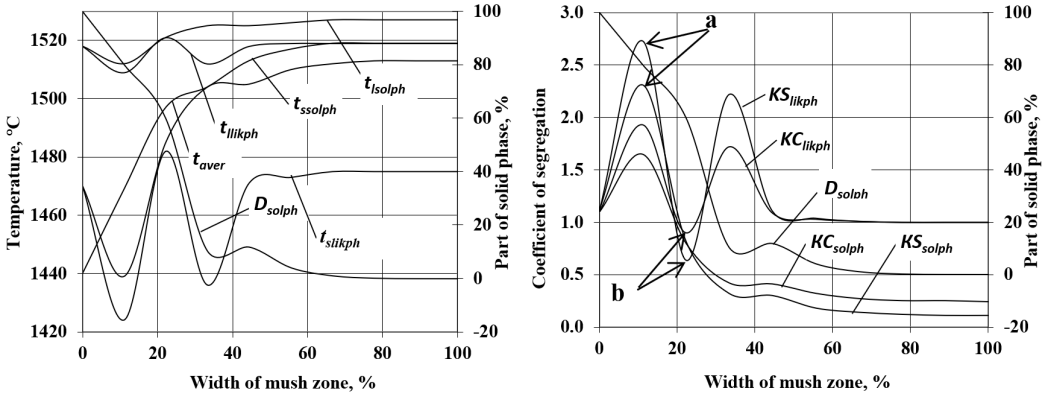

Fig. 5. Distribution of settlement parameters on width ingot's mushy zone in steel with [C]=0.1%.

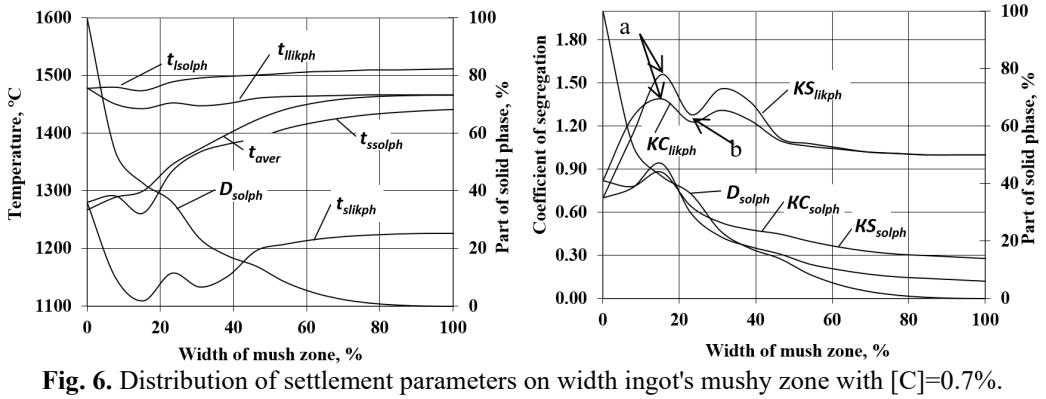

Fig. 6. Distribution of settlement parameters on width ingot's mushy zone with [C]=0.7%.

The analyses in Figures 5 and 6 show that the dissolved liquid steel impurity distribution across the mushy zone width are not exponential according to the quasi-equilibrium mushy zone theory but have wavy character. Figures 5 and 6 show high impurities in concentration areas along the liquidus line and low impurities in concentration areas shown by arrows a and b in figures. Thereafter, conditions can be set for the formation of impurity foliation associated with melt solidification in areas with increased concentration with overcooling that can be often seen in reality.

The decreasing distance between dendrite arms and the increasing solid phase shared in these areas slow down the motion of segregates inside the mushy zone, for example, increasing D_{solph} in the 40–50% mushy zone width (**Figure 5**). This is the reason for segregated bands appearance.

The impurity concentration and the corresponding temperature curve fluctuations in the solid phase across the mushy zone width are less observed. These zones have directed mass transfer because impurities have not enough time for redistribution between the solid and liquid phases considering the distribution coefficient.

The decreasing impurity concentration in the initial melt is the reason that the mushy zone width decreases and the impurity speed motion increases. The reason is that the impurity wave amplitude distribution in the liquid phase of the mushy zone during solidification time is higher for billet with the 0.1% carbon content (**Figure 5**) than for billet with the 0.7% carbon content (**Figure 6**). Accordingly, the concentration of segregator changes with liquid phase solidus and liquid temperature curves also changes, and the solid phase part inside the mushy zone changes more sharply as compared to billet with 0.7% carbon content.

As the distribution of segregators does not remain stable during time and space inside the mushy zone, the possible concentration of segregators increases in mushy zone parts and higher solid phase parts. Then, the growth rate of the solid phase part decreases and the concentration of segregators redistributes. This effect is more typical for steel grades with small mushy zone width, for example, for steel grades 10 or 20 according to GOST 1050–88. The reason is that the impurity segregation level in the solidified ingot with lower initial impurity contents is lower as compared to ingot with higher initial impurity concentrations. It is confirmed by the final impurity distribution across billet with dimensions 400 × 400 mm and the 0.7% carbon content transversal section as represented in **Figure 7.**

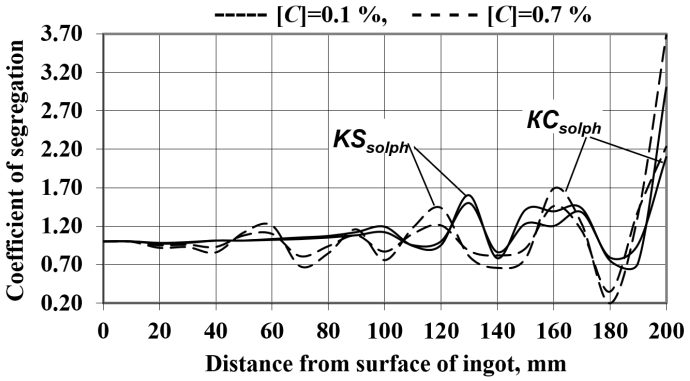

Fig. 7. Segregation indexes distribution in a solidified billet with section 400 × 400 mm with [C]=0.7%.

The carbon and sulfur segregation indices of the curved phase synchronism are not found on some parts of the billet transversal sections (**Figure 7**). This is the result of different speeds of different impurities inside the mushy zone. The reason is that the distribution impurity extrema do not coincide with the solidified ingot. The average temperature curve is calculated on the basis of the equilibrium of the solid and liquid phases and D_{solph}, considering curves are not uniform.

The t_{aver} change corresponds to the change in the solid phase part (**Figures 5** and **6**). In **Figure 5**, some parts of the mushy zone have negative temperature gradient and this effect agrees with experimental data [33]. This effect is

associated with diffusion undercooling and diffusion undercooling as a result of impurity segregation decreases in this part of the mushy zone. The decrease in impurity concentrations defines the solidus and liquidus temperature changes and average equilibrium temperature.

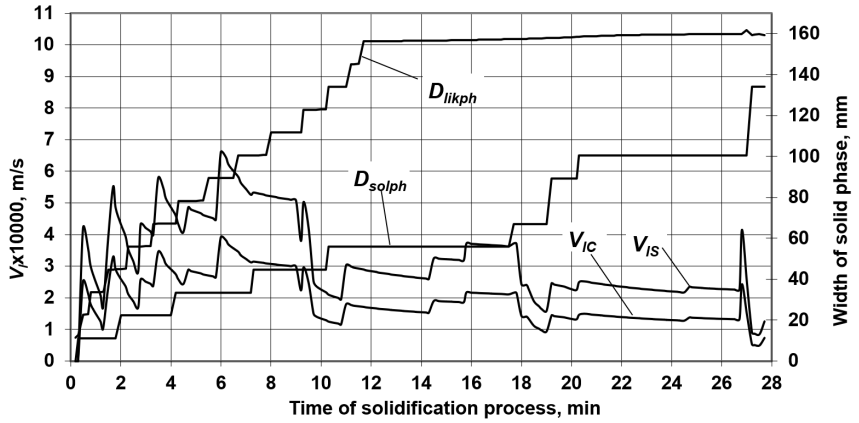

Fig. 8. Parameters of the crystallization process of ingot (335 × 400 mm) with [C]=0.6%, [S]=0.01%, [Mn]=0.5%.

Segregators with increased carbon and sulfur contents and average motion speeds in the calculated time interval for billet with section 335 × 400 mm and a casting speed of 0.6 m/min are represented in **Figure 8** (D_{likph}, D_{solph} are the ingot skin width on the isoliquidus and isosolidus lines, respectively). The changes in the speed of motion segregator have not found to be steady at the solidification time. The reason is the influence of different parameters and it is impossible to consider it in this mathematical model. Therefore, solid phase parts, segregation ratio, and the analysis of motion speeds of segregators help to conclude that (1) the motion speed of segregators across the mushy zone width at solidification time are not steady; (2) impurity concentration minima in the calculated point of the mushy zone coincide with the impurity motion speed maximum; (3) the motion speed of segregators increases without an increase in the solid

phase part in the isoliquidus direction; (4) segregator motion speed maximum and minimum coincide with the inner space of the mushy zone; (5) the segregation ratio minimum coincides with the solid phase part minimum and the segregation ratio maximum coincides with the solid phase part maximum if the motion of segregators is a finite velocity and coincides inversely if the velocity is equal to zero.

The similar investigations of segregation for other steel grades and other billet dimensions show common results, but the investigated solidification parameters change for every situation strictly and individually. The reason is that external action to the solidified ingot corresponds to the calculated time intervals and accordingly the wave motion of segregator inside the mushy zone is found to be reasonable. Mathematical statistics are used for calculating the impurity concentrations influence segregation and motion type and speed.

Numerical experiments are carried out by using the method of the orthogonal central composite plan [34]. The carbon content changes from 0.2% to 0.6%, the sulfur content changes from 0.01% to 0.04%, and the manganese content changes from 0.5% to 1.5%. The maximum (max) of the segregation level for the corresponding impurities after solidification is used as a response function. The statistical analysis of the results provides the next regression dependences (R_k is the correlation coefficient):

$$KS_{\text{solph}} = -0.014 + 2.06KC_{solph},\ R_k = 0.96; \qquad (18)$$

$$KC_{\text{solph}} = 0.677 + \frac{0.0485}{[C]} + 1.84 \cdot 10^{-8+[C]\frac{[Mn]}{[S]}},\ R_k \approx 1. \qquad (19)$$

The calculations show the nonlinear type of carbon content and the [Mn]/[S] ratio influence to carbon and sulfur segregation coefficients. Experimental data confirm these calculations.

According to our calculations, sulfur segregation decreases considerably as the carbon content decreases. Experimental data confirm our calculation results and the correctness of numerical simulation propositions.

We determined that segregator's motion average and maximum velocities have next statistical association with the initial impurity concentrations:

$$V_{\mathrm{C}}^{\mathrm{aver}} = 4.386 - 5.575[\mathrm{C}] + 2.73 \cdot 10^{-7} \mathrm{e}^{-[\mathrm{C}]\frac{[\mathrm{Mn}]}{[\mathrm{S}]}},\ R_k = 0.72 \qquad (20)$$

$$V_{\mathrm{S}}^{\mathrm{aver}} = 12.75 - 6.1\mathrm{e}^{[\mathrm{C}]} + 4.68\mathrm{e}^{[\mathrm{C}]\frac{[\mathrm{Mn}]}{[\mathrm{S}]}},\ R_k = 0.71; \qquad (21)$$

$$V_{\mathrm{C}}^{\max} = 3.58 + \frac{0.434}{[\mathrm{C}]},\ R_k = 0.90; \qquad (22)$$

$$V_{\mathrm{S}}^{\max} = 5.975 + \frac{0.693}{[\mathrm{C}]},\ R_k = 0.73. \qquad (23)$$

We determined that impurity segregation velocity ratio is variable and depends on the initial chemical composition of the melt. The statistical analysis of results provides the next regression dependences:

$$\frac{V_{\mathrm{S}}^{\mathrm{aver}}}{V_{\mathrm{C}}^{\mathrm{aver}}} = 1.707 + 0.053\ln[\mathrm{C}],\ R_k = 0.99; \qquad (24)$$

$$\frac{V_{\mathrm{S}}^{\max}}{V_{\mathrm{C}}^{\max}} = 1.594 - 2 \cdot 10^{-17+\frac{[\mathrm{Mn}]}{[\mathrm{S}]}} + 0.12[\mathrm{C}] + 2.76 \cdot 10^{-4}[\mathrm{C}]\frac{[\mathrm{Mn}]}{[\mathrm{S}]},\ R_k \approx 1. \qquad (25)$$

Accordingly, the dependences in Eqs. (24) and (25) show that the microblast motion speed with high sulfur concentration increases more as compared with microblast motion speed with high carbon concentration if the carbon content increases. The reason is that impurity concentration extrema do not coincide and data in an earlier study [11] confirm this effect. The probability of effect increases if the carbon concentration also increases.

In an earlier study [35], it was stated that the processes of volume solidification with a zone of equiaxed crystals (EZ) begin only when the mushy zone occupies all non-solidified part of the ingot. We carried out the corresponding numerical analyses on the basis of the presented mathematical model of impurity segregation. The billet formation simulates according to plant conditions. The comparison of our calculations with literature and practical data shows that the skin zone (SZ) formation finishes at the same time when impurity filtration begins. Moreover, columnar crystal zone (CZ) formation finishes at the same time when impurity filtration finishes. The determination of the parameters of structural zones is not difficult. SZ represents the forest of dendrites extended to the iso-liquidus direction. Impurities directed with mass transfer are created inside SZ and this process is started in the presented mathematical model without any difficulty. Conditions for the directed mass transfer disappear when volume solidification and EZ formation start. This affects our ingot concentration and the thermal condition model is also fixed easily.

The calculated results of the structural zone width according to our model and dependences according to earlier works [2,3] and practical measures are presented in Table 2. All calculations are carried out experimentally under the same conditions. Statistically compared calculation results and experimental data show that our model calculation results are more accurate calculations for ingot macrostructure in all cases. The presented model can not only be used for the prediction of segregator's distribution but also for the prediction of ingot macrostructure.

Table 2. Theoretical and practical data are a comparison of the width of structural zones.

Steel grade, section (mm)	**Structural zone**	**Width of zones, mm**		
		by the author's method	**By earlier techniques [2,3]**	**Practical data**
St20/St45, 335×400	SZ	13.3/13.3	26.7/26,7	12–17/12–17
	CZ	106.7/80	106.6/90	86–122.5/79–137
	EZ	95/148.4	68.4/95	81–112/35–160
St20/St45, 160×160	SZ	12.3/12.3	26.7/26.7	8–12/8–12
	CZ	40.9/35.7	32.25/26.6	34–57/20–40
	EZ	53.6/64	42.1/53.4	22–75/60–93

The numerical analysis of the structural zone width (D_{SZ}, D_{CZ} , D_{EZ} ,%) from the carbon content ([C] = 0.1–0.7%) and from the half of billet thickness (h = 0.075–0.2 m) is carried out according to the rotatable central composite planning of experiments. All other conditions are the same. We predicted the billet structure for a specific continuous caster and determined that the structural zone parameters depend on the billet section, carbon content, and casting speed. We determined the next regression dependences as follows:

$$D_{\mathrm{SZ}} = 32.343 - 268.22h^2 + 709.9h^2 - 4.02[\mathrm{C}] + 9.34[\mathrm{C}]^2,\ R_k{\approx}1; \quad (26)$$

$$D_{\mathrm{CZ}} = 136.65 - 47.18[\mathrm{C}]^2 - 1774.17h^2 v_{\mathrm{cast}}^2,\ R_k{=}0.85; \quad (27)$$

$$D_{\mathrm{EZ}} = 35.608 + 2706.9h^2 + 42.9[\mathrm{C}]^2 - 535.04h,\ R_k{=}0.87. \quad (28)$$

We determined that D_{SZ} increases, if [C] also increases. The heat of phase transition decreases if the carbon content increases. D_{SZ} decreases if increase in h is associated with the increase in the metal enthalpy.The derived results are in close approximation with calculated data [2,3] and experimental data [36].

Therefore, the presented mathematical model can be used for the heat and mass transfer analysis of continuous casting billet solidification time and can predict temperature and concentration billet conditions for different continuous casting parameters at every time station.

4. Conclusion

The theory of melt solidification with different chemical compositions has further scope to be developed in future. This theory considers microblasts with different chemical compositions in the solidifying melt that is found important for manufacturing metal production with minimal segregation. The presented model conceptions for analyzing the finite state of the real continuous casting billet are confirmed by advanced methods.

On the basis of the results of the presented model for heat and mass transfer at solidification time, it was established that impurities, temperatures, and solid phase part distributions inside the mushy zone on time and space are nonstable and possess wave-type structure. The segregation level, concentration extremum divergence of different segregators, and impurity motion velocities in the mushy zone depend on the main form of the steel chemical composition and billet section. The quantitative evaluation of the impurity distribution inside the mushy zone allows determining continuous casting technological parameters for billet manufacturing with minimal segregation on a scientific basis.

Acknowledgments

The authors gratefully acknowledge the support from the Major Technology Innovation of Hubei Province under grant No. 2016AAA022 and the National Material Environment Corrosion Platform “Basic Research on the Key Technology of Corrosion and Protection of Marine Engineering Equipment Materials” (Grant No. 2014CB643300).

References

1. V.T. Borisov, The theory of steel ingot mushy zone, Moscow, Metallurgy, 1987, 224 p.
2. I.N. Golikov, S.B. Maslenkov, Dendrite segregation in steels and alloys, Moscow, Metallurgy, 1977, 224 p.
3. V.A. Efimov, Steel casting and solidification, Moscow, Metallurgy, 1976, 552 p.
4. Y. Natsume, K. Ohsasa, Three-dimensional Cellular Automaton Model for the Prediction of Microsegregation in Solidification Grain Structures, ISIJ International, Vol. 54 (2014), No. 2, pp. 415–421.
5. D. Jiang, M. Zhu, Center Segregation with Final Electromagnetic Stirring in Billet Continuous Casting Process, Metallurgical and Materials Transactions B, V. 48B, February 2017, pp. 444–455.
6. D. Jiang, W. Wang, S. Luo, C. Ji, M. Zhu, Mechanism of Macrosegregation Formation in Continuous Casting Slab: A Numerical Simulation Study. Metallurgical and Materials Transactions B, V. 48B, December 2017, pp. 3120–3131.
7. N.T. Gugcov, Main questions of steel ingot study, Proceedings Steel ingot, Moscow, Metallurgizdat, V.1, 1952, pp. 11–20.
8. P.A. Dudovcev, Periodicity properties in steel ingot, Moscow, Metallurgizdat, 1949, 67 p.
9. K. Miyazawa, K. Schwerdtfeger, Macrosegregation in continuously cast steel slabs: preliminary theoretical investigation on the effect of steady state bulging, Arch. Eisenhutten, 1981, 52(11), pp. 415–422.

10. A.M. Skrebcov, Convection and solidification steel melt in to ingot and casting, Moscow, Metallurgy, 1993, 144 p.
11. B.B. Gulyaev, Steel solidification and inhomogeneity, Moscow, Metallurgizdat, 1950, 228 p.
12. R. Mehrabian, M. Keane, M.C. Flemings, Inter-dendritic fluid flow and macrosegregation; influence of gravity, Metallurgical and Materials Transactions B, 1970, 1(5), pp. 1209–1220.
13. J. Ni, C. Beckermann. A Volume–Averaged Two–Phase Model for Solidification Transport Phenomena, Metall. Trans. B, 1991, 22B, pp. 349–361.
14. A.M. Screbcov, L.A. Dan, V.V. Kylochkin, New vision to chemical elements concentration periodicity changing on steel ingot radius, Universities news, Ferrous metallurgy (Izvestiya vuzov. Chernaya metallurgia), 1991, # 7, p. 106.
15. A.M. Screbcov, Impurities periodically distribution on steel ingot radius, Foundry processes (Processylitya), 1994, # 3, pp. 16–23.
16. A.H. Urazgildeev, S.N. Pronskih, A.A. Alymov, Influence of chemical elements concentrations to segregation velocity at ingots solidification, Universities news, Ferrous metallurgy (Izvestiya vuzov. Chernaya metallurgia), 1981, # 9, pp. 49–52.
17. E.A. Kazachkov, S.L. Makurov, Big ingots chemical inhomogeneity formation and optimization ingots parameters, Foundry processes (Processy litya), 1996, # 1, pp. 35–44.
18. E.J. Pickering, Macrosegregation in Steel Ingots: The Applicability of Modelling and Characterisation Techniques, ISIJ International, Vol. 53 (2013), # 6, pp. 935–949.
19. M.C. Flemings, Our Understanding of Macrosegregation: Past and Present, ISIJ International, Vol. 40 (2000), # 9, pp. 833–841.
20. M. Miyazaki, T. Murao, K. Isobe, Formation Mechanism and Modeling of Centerline Segregation, Nippon Steel Technical Report, #104, August, 2013.
21. E.J. Pickering, Macrosegregation in Steel Ingots: The Applicability of Modelling and Characterisation Techniques, ISIJ International, Vol. 53 (2013), # 6, pp. 935–949.
22. N.M. Belyaev, I.N. Manusov, I.K. Karimov, Using the methods of elementary heat balances to thermal conductivity with difficult boundary conditions decisions, Dnepropetrovsk, Dnepropetrovsk state University, 1985, 128 p.
23. A.P. Ogurcov, A.V. Hress, Steel continuous casting, Dnepropetrovsk, System technologies, 2002, 675 p.
24. Sh. Lei, J. Zhang, X. Zhao, K. He, Numerical Simulation of Molten Steel Flow and Inclusions Motion Behavior in the Solidification Processes for Continuous Casting Slab, ISIJ International, Vol. 54 (2014), No. 1, pp. 94–102.
25. V.T. Sladcoshteev, R.V. Potanin, O.N. Suladze, Continuous casting on radial casters, Moscow, Metallurgy, 1974, 288 p.
26. V.V. Savchenko, A.M. Kolotov, E.P. Lobanov, Heat work of radial caste for big sections billets casting, Proceedings, Vol. 5, Moscow, Metallurgy, 1978, pp.79–83.
27. V.V. Sobolev, P.M. Trefilov, Continuous casting solidification thermophysics, Moscow, Metallurgy, 1988, 160 p.
28. Yu.A. Samoylovich, Using computer for solidification ingot tasks decision, Moscow, Metallurgy, 1988, 182 p.
29. M.Ya. Medzhibozhskij, P.S. Harlashin, Theoretical basis of steelmaking, Kiev, NMK VO, 1983, 276 p.
30. E.A. Kazachkov, V.A. Fedorov, The investigation of carbon segregation at big ingots solidificstion, Proceedings VI Conference: Steel ingots problems, Moscow, Metallurgy, 1976, pp. 132–135.
31. O.S. Logunova, I.M. Devyatov, I.M. Yachikov, Numerical simulation of continuous casting ingots macroscopic parameters, Universities news, Ferrous metallurgy (Izvestiya vuzov. Chernaya metallurgia), 1997, # 2, pp. 49–51.
32. B.A. Movchan, Microscopic inhomogeneity in casting alloys, Kiev, Gosisdat, 1962, 340 p.
33. V.M. Scheglov, I.N. Primak, I.M. Stas', Temperature fields in solidificating steel ingots, Proceedings, International Research Congress: Metals melting, treatment and casting, Kiev, 2006, pp. 17–18.
34. S.A. Ayvasyan, I.S. Enyukov, L.D. Meshalkin, Applied statistics, Dependences investigations, Reference book, Moscow, Finances and statistics, 1985, 487 p.
35. V.M. Kitayev, V.N. Guschin, The investigation mushy zone extent at ingots solidification, Proceedings, Ingots and castings structure control, Gor'kij, Gor'kij Politechnic Institute, 1984, pp. 27–34.
36. V.S. Luchkin, S.A. Vorobej, G.V. Levchenko, Continuous casting billet with different sections quality specificity, Metal and foundry of Ukraine (Metal and litye Ukrainy), 2005, # 5, pp. 30–33.